




# An Experimental Study of Plasma Cracking of Methane Using DBDs Aimed at Hydrogen Production

Ruggero Barni<sup>1</sup>  · Roberto Benocci<sup>2</sup> · Nicolò Spinicchia<sup>3</sup> · H. Eduardo Roman<sup>2</sup> · Claudia Riccardi<sup>1</sup>

Received: 3 August 2018 / Accepted: 15 October 2018 / Published online: 23 October 2018  
© Springer Science+Business Media, LLC, part of Springer Nature 2018

## Abstract

We report the results of an experimental campaign about the production of hydrogen from methane cracking using a non-thermal plasma. Experiments have been performed using a nanosecond pulse high-voltage generator in a cylindrical dielectric barrier electrode setup. Our experiments show that high methane conversion could be achieved by pulsed electrical discharges in DBD configuration. Conversion could be as high as 60%, with a hydrogen yield of about 25%. The energy costs lie in the range 30–40 eV for molecule. Another set of experiments using a traditional sinusoidal dielectric barrier discharge reactor suggests that argon dilution could improve the performances of plasma methane reforming. A similar suggestion could be inferred by analyzing the results of numerical simulations of the gas-phase chemical kinetics evolution under pulsed electrical discharge conditions.

**Keywords** Plasma discharges · Atmospheric pressure plasmas · Dielectric barrier discharges · Hydrogen reformer · Methane cracking

## Introduction

Hydrogen was considered the most promising source to be used in clean energy systems for transportation, distributed heat and power generation or energy storage [1–3]. The most direct way of hydrogen production is through hydrolysis. Despite its very high selectivity (see below for definition), about 99%, and simplicity, the main drawback lies in the energy costs, mainly electricity, which are even for the best devices in the order of 144 kJ/g of hydrogen produced [4]. The reformation of various hydrocarbons, such as methanol, methane and gasoline, has been considered as possible alternative hydrogen sources. In such

---

✉ Ruggero Barni  
ruggero-barni@mib.infn.it

<sup>1</sup> Dipartimento di Fisica G.Occhialini, Università degli Studi di Milano-Bicocca, p.za della Scienza 3, 20126 Milan, Italy

<sup>2</sup> Dipartimento di Scienze dell'Ambiente e della Terra, Università degli Studi di Milano-Bicocca, p.za della Scienza 1, 20126 Milan, Italy

<sup>3</sup> Istituto di Fisica del Plasma, CNR Consiglio Nazionale delle Ricerche, Via Cozzi 53, 20125 Milan, Italy

cases, hydrogen production is generally endothermic. As a reference, the steam reformer reaction  $\text{CH}_4 + \text{H}_2\text{O} \rightarrow 3\text{H}_2 + \text{CO}$  has an enthalpy  $\Delta H = -206.1$  kJ for each converted  $\text{CH}_4$  mole [5]. The main reforming technology is catalytic reforming, which has been studied by many laboratories and car manufacturers for about 15 years and offers good efficiency. High conversions (up to 77%) can be achieved, with  $\text{CO}_2$  as the main by-product [6]. Nevertheless, this technology has some limits concerning dynamics, durability, cost and compactness [7]. The formation of greenhouse gases is another drawback. As a viable alternative it was suggested to use the plasma state as a reactive environment [8]. The most direct way is to use a thermal plasma source, since this could provide the hot gas-phase needed to overcome endothermic reactions [9–12]. However, most chemical reactions in a plasma happens generally under non-thermal equilibrium conditions. This mitigates the need of heating of the gas-phase. In particular, a non-thermal plasma reactive media could be considered for local generation because energy is concentrated in a minority population of high energy electrons, needed to sustain the plasma and promoting plasma dissociation of hydrogen atoms bound in molecules [13, 14]. Formation of molecular hydrogen can be achieved on short time scales and without substantial heating of the gas-phase. This also addresses the problem that pure hydrogen feeding is relatively difficult for practical applications and can result in safety issues and storage problems [15]. Indeed, this boosts interest in local production or in hydrogen enrichment directly on board.

The limitation of working near or at atmospheric pressure reduces the choice of plasma sources. The more viable solution lies in the use of insulating barriers to quench discharges before a thermal plasma is formed. This wide class of plasma devices can be categorized generally as dielectric barrier discharges (DBD), about which excellent reviews already exist in the literature [16].

Although several hydrocarbon precursors could be considered and have been actually proposed as plasma reformers, methane should be taken into account as the most neat and simple choice in order to evaluate different proposed pathways. We could also remind that argon dilution of methane in a plasma gas-phase leads to better conversion and selectivity, as it was reported in the framework of plasma chemical vapor deposition processes aimed at diamond-like thin film growth [17]. Another important issue worthwhile mentioning, regards the plasma potential capability to dissociate complex hydrogen rich mixtures in different phases (e.g. volatile organic compounds VOCs) and, therefore, turn industrial by-products into sustainable resources [18].

Here, we present the results of an experiment useful to gain a perspective about the use of DBD as a source for hydrogen reforming. After a description of the experimental setup and diagnostics, we discuss the results of experiments obtained with a pulsed DBD power supply. Then, we address the suggestion of improving selectivity by using argon dilution in a more traditional sinusoidal DBD. Finally, we discuss also briefly the mechanisms leading to hydrogen formation in the gas-phase by performing some specific simulations of the chemical kinetics in the plasma.

## Experimental Set-Up

The first set of experiments were performed at the I.F.P. (Istituto di Fisica del Plasma)-CNR Laboratories in Milan [19]. The layout of the plasma reactor is displayed in Fig. 1a. The reactor is made of a quartz cylindrical tube (inner diameter 32 mm, height 210 mm and thickness 2 mm). Inside and coaxially, an aluminum cylinder is positioned which acts

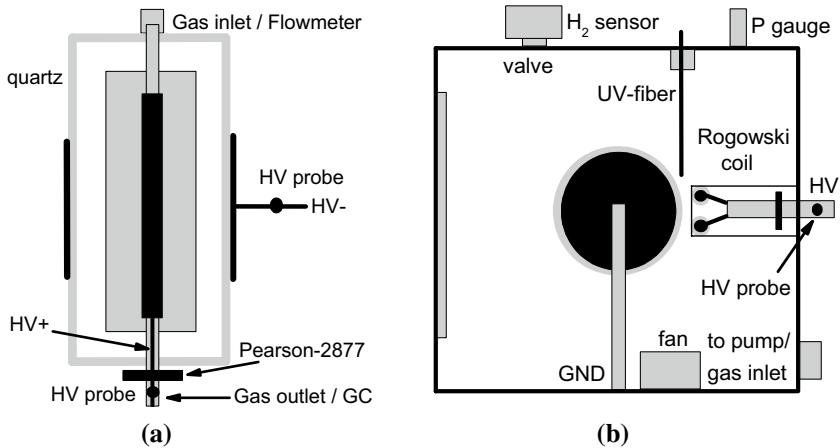


**Fig. 1** Schematic view of the experimental setup and diagnostics of the plasma reactors: Milano CNR Laboratory (a), Milano-Bicocca Laboratory (b)

also as the internal electrode (height 170 mm, diameter 25–28 mm). Outside the quartz tube a copper strip is glued on the external surface (height 40–100 mm) which acts as external electrode and ensures an almost ideal cylindrical geometry of the driving electric field in the discharge region. In the experiments, the external electrode height and the internal electrode diameter were varied to optimize reforming efficiency as discussed below. The electrode system capacitance is dominated by the gas gap contribution: a value of 16 pF was estimated for an external electrode height of 80 mm and an internal electrode diameter of 25 mm (quartz tube contribution to capacitance was about 143 pF, while that of the gas gap 18 pF). Two Teflon plugs with silicon gaskets ensure sealing from external atmosphere. The plugs houses also the gas inlet and outlet as well as the HV feedthrough. Methane flow was set to 100 sccm and the working pressure is 1 bar. During the discharge operation, the electrodes temperature maintained always below 200 °C. So we avoid any substantial heating of the final gas-phase. Depending on the different discharge region gap distances, the flow velocity varied between 5 and 9 mm/s. This implies that the residence time in the discharge region spans between 4.5 and 19 s (accounting also for the different external electrode heights). The total residence times in the reactor varied between 19 and 34 s. Both times are quite smaller when compared with the diffusion time along the flowlines, which turns out to be longer than a 100 s according to a rough estimate based on an approximation discussed by Chantry [20]. This means that the reactor always operates in the so-called plug-flow regime [21]. That is, the gas-phase gets only limited mixing along the streamlines. On the other hand, the diffusion time across the gap is much shorter, between 18 and 62 ms, which allows the gas-phase mixing along the electric field lines, thus mitigating any effect due to the non-uniformity of the electric field because of the cylindrical discharge region.

The discharge is driven by a HV pulse generator (HVPG-FPG 30 model by FID GmbH) which provides an approximately square bipolar voltage pulse with a duration of about 60 ns. HV peak-to-peak amplitude could be regulated between 6 and 30 kV (nominally on a 1 k $\Omega$  load). Repetition frequency could be set between 15 and 100 kHz. Actually, the generator is composed by four modules (each capable up to  $\pm 7.5$  kV) which could be connected in order to reach the maximum bipolar pulse of 30 kV. The actual voltage on

both electrodes was monitored by two equal HV probes (P6015A by Tektronix, bandwidth 75 MHz) on the high impedance input of a scope (TDS 714L by Tektronix). The discharge current was measured by an inductive current probe (model 2877 by Pearson, 100 A range, bandwidth 300 Hz–200 MHz, rise time 2 ns) connected to another input of the same scope. The probe was inserted along the internal electrode side of the supply circuit. The numerical integration of the product between the instantaneous values of the potential difference and the current allows to calculate the average electrical power exerted by each discharge. It is also clear that the high repetition frequency (discharge time lapse varied between 10 and 67  $\mu$ s) implies that the gas molecules have the possibility to interact with several hundred thousand discharges before exiting the reactor, therefore making the final gas-phase products uniform as a result of fluctuations arising from discharge repetitions.

The analysis of the gas-phase composition produced by plasma processing of the methane flow was performed by means of a gas chromatograph (GC) (GC-1000 DPC by DANI Instruments). This was equipped with two columns, the first better suited for hydrogen (Molsieve CP7538 by Varian) whereas the second was better suited for hydrocarbons (PoraPLOT-Q CP7554 by Varian). The GC was equipped also by two detection system, a PT100-FID 86/C flame ionization sensor and an OPT270 Micro-TCD thermo-conductivity detector. Calibration of the GC was performed using two prepared gas mixture cylinders ( $H_2/CH_4/C_2H_6/C_2H_4$  quaternary blend in different concentrations). The total amount of gas sampled to perform a complete analysis was about 3 mL.

The second set of experiments has been performed in the PlasmaPrometeo Laboratories at Milano-Bicocca University. The experimental setup of the plasma device is shown in Fig. 1b. The plasma reactor has been described at length in our previous papers [22, 23]. The electrical discharge happens in the gap between a couple of rod electrodes, fed by the same HV signal, and a larger rotating cylinder, which is grounded. The two rod electrodes (220 mm long, 8 mm diameter) are coated with sintered  $Al_2O_3$  dielectric ceramic (thickness 2 mm). They are held parallel and 20 mm apart. The two-rod system is aligned and maintained at a fixed distance, here set to 1 mm, from a stainless steel cylinder (diameter 150 mm, height 295 mm) coated with the same dielectric material (thickness 5 mm). The cylinder can also rotate around its axis at a desired pre-fixed speed. In the present configuration, the electrodes has a capacitance of 52 pF and are placed inside a vacuum chamber in order to be able to operate under controlled atmosphere and gas flow. The cube-shape vacuum chamber, with 42 cm side, is evacuated by a double-stage rotary pump (SD-301 by Varian), reaching a residual pressure of about 0.3 Pa [23]. After evacuation, the pumping outlet is closed and the process gas-phase is prepared. This is achieved by filling the chamber through a micrometer valve using a high purity cylinder, loaded with a 5% methane in argon. The gas-phase was filled up to a pressure slightly less than the atmospheric one (recorded by a capacitive gauge CMR361 by Pfeiffer). More diluted methane gas-phases can be obtained by adding also high purity argon from another cylinder and monitoring the partial pressures. The total volume of the gas-phase was estimated as 47.4 L (reduced from the original vacuum chamber volume by partial covering the device inner walls with low out-gassing ceramic tiles). A rough estimate suggests that the diffusion time in the device is of the order of 115 s [20]. The reactor operates in the well-mixed regime as soon as the plasma exposure time exceeds a few minutes [21]. However, a mixing fan was inserted in the vacuum chamber, which could be switched on to eventually level out the gas-phase.

A Laboratory Corona Station V20 by Tigres GmbH was used to ignite the electrical discharge [22]. The power supply provides an alternating high voltage signal. This voltage signal flows in the primary circuit coil of an air cooled transformer (ATV-20, 2.5 kW by Tigres GmbH). The secondary HV-end coil is connected in parallel to both the two-rod

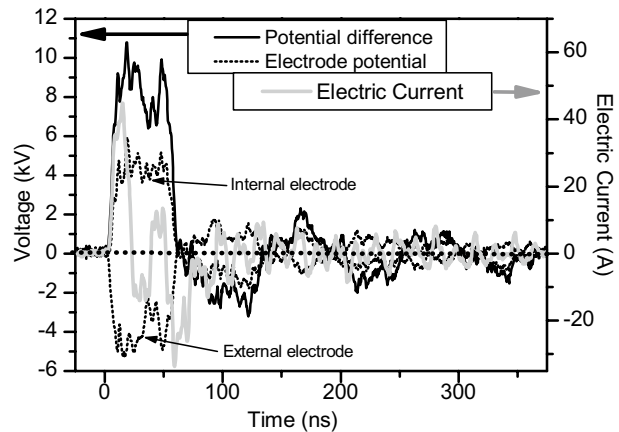
electrodes. The other grounded end of the coil is connected with the rotating cylinder. As a result, an alternate electric field appears in the gap between the electrodes. The HV frequency can be varied between 18 and 50 kHz. In the normal operating mode, the frequency is automatically adapted by a feed-back loop in order to provide a constant pre-determined output power level in the range 60–300 W [22]. The device could also work in pulsed operation mode. A P6015A Tektronix probe with a bandwidth of 75 MHz was used to measure the HV signal directly at the vacuum feed-through which connects the two-rod electrodes. A Rogowski coil, connected to the same HV line [24, 25] records the entire current flowing through the discharge gap. A proper design of the coil and a calibration allowed a bandwidth comparable with the HV probe to be obtained, as discussed elsewhere [26]. A fast scope (MSO-8104A, 4 GHz, 4 MS by Agilent) was used to record simultaneously voltage and current signals. The current signal was then analyzed using a Fast Fourier Transforms software to take into account the calibration and to remove the low frequency signals corresponding to the displacement current [26]. As a result, we obtained time series containing only the signal of the micro-discharges current pulses. Besides electrical measurements, the discharge was characterized through Optical Emission Spectroscopy (OES) [27]. Light emitted locally from the discharge gap was collected by an UV enhanced sensitivity 200  $\mu\text{m}$  optical fiber by Avantes (see Fig. 1b) and analyzed by a CCD spectrometer (AvaSpec-2048 by Avantes), with a holographic grating (300 lines/mm, blazed at 300 nm) and a 10  $\mu\text{m}$  slit. The instruments cover the UV–Vis–IR range between 180 and 1150 nm, with a resolution around 0.8 nm [28]. It allows mainly the identification of some radicals and molecules produced in the discharge region, by recording the full visible emission spectra.

Hydrogen production was estimated by means of a hydrogen sensor, using a tin dioxide semiconductor probe (TGS 821 by Figaro Inc.). The sensor is sensitive to concentrations between 10 and  $10^4$  ppm. Its selectivity is also high, providing negligible signal in presence of methane as well as other hydrocarbons even in large concentrations. The sensor was however calibrated before the experiments using a high purity hydrogen cylinder to prepare suitable diluted mixtures in air and argon [29]. The sensor was then inserted into a separated section of the reactor (see Fig. 1b) to protect it during the evacuation, filling and plasma discharge phases of the treatment. After the methane exposure to the plasma discharge, the gas mixture is allowed into the sensor region and the hydrogen concentration is measured. The sensor output reaches equilibrium in about 15 min, remaining stable even for several hours. The hydrogen concentration in the final gas-phase can be reduced below the maximum tolerance of the sensor by pumping away part of the gas and mixing the rest with inert argon. In this way, hydrogen concentration above 1% have been measured too.

## Experimental Results

A typical plot of the electrical discharge parameters during the first set of experiments is shown in Fig. 2. The fairly symmetric bipolar HV pulse has a duration of 50.2 ns (FWHM) and an average amplitude of  $8.2 \pm 1.2$  kV. The current pulse is much faster with a duration of 13.4 ns (FWHM), somewhat triangular, with a peak of 44.9 A. At the end of the HV pulse, during the switch-off, a weaker inverse current pulse is recorded too (peak amplitude  $-33.7$  A and duration 14.6 ns). Before that and after the main pulse, some rebounds in the current signal are observed. They are mostly due to the finite, not so-high bandwidth of the current probe. On the other hand, the rebound in the HV signal (maximum amplitude  $-3.2$  kV and

**Fig. 2** Voltage and current pulses measured in a 2 mm gap discharge



duration 46.8 ns) depends on the actual nature of the load, more precisely on the mismatch between the power supply and load impedances. The current signal, however, shows that this is not matched by any significant electrical current, ruling out either any spurious discharge or the achievement of breakdown conditions. The integrated main current spike contains a total charge of about 550 nC. This corresponds to an accumulation of an excess positive charge towards the quartz internal surface of the reactor. Such a charge gets almost completely discharged after the end of the return current pulse. Similarly, integrating the product between the electric current and the potential difference across the electrodes, one gets about 110 W, as average power adsorbed by the discharge. Such a value is mainly due to the main current spike (roughly 80%).

In Table 1, we report a typical GC plot analysis of the final gas-phase 1. Besides the calibrated peaks, we observe the presence of several other hydrocarbons, the most relevant being ethyne (acetylene,  $C_2H_2$ ) and propane ( $C_3H_8$ ), whose area, however, is generally small. Lacking a calibration they were ignored. As discussed in [29], their contribution is minor and, therefore, not affecting the main conclusions of our experimental campaign. A quantitative evaluation of the hydrogen yield,  $Y_{H_2}$  could be obtained by considering the ratio between the number of moles of hydrogen produced and that of methane introduced:

$$Y_{H_2}(\%) = \frac{1}{2} \cdot \frac{\text{moles of } H_2 \text{ out}}{\text{moles of } CH_4 \text{ in}} \cdot 100 \quad (1)$$

**Table 1** Analysis of a typical chromatogram measured by the GC during experiments with peaks identification and measure of the concentrations

Peak no.	Retention time (min)	Amount ( $\mu\text{mol}$ )	Amount (%)	Peak identification
1	5.15	70.18	56.0	$H_2$
2	7.65	1.81	1.4	$C_2H_4$
3	7.95	0	0	–
4	9.09	6.85	5.5	$C_2H_6$
5	38.54	46.55	37.1	$CH_4$
Total		125.39	100.0	

The coefficient 1/2 accounts for the four hydrogen atoms available in each methane molecule [30]. The same ratio could be defined for each chemical species detected in the outlet flow. For hydrocarbons such as C<sub>2</sub>H<sub>6</sub> and C<sub>2</sub>H<sub>4</sub> the yield just coincides with such a ratio. Instead of the yield, for methane it is more significant to consider the percentage variation of the amount of methane before and after the reactor, a quantity which is referred to as the conversion fraction [30]. The methane conversion,  $X_{CH_4}$  is calculated according to the following relation:

$$X_{CH_4}(\%) = \frac{\Delta(\text{moles of } CH_4 \text{ in} - \text{moles of } CH_4 \text{ out})}{\text{moles of } CH_4 \text{ in}} \cdot 100 \tag{2}$$

A typical trend of the obtained yield/conversion is reported in Fig. 3 as a function of the electrical power adsorbed by the discharges, for two similar configurations, differing for the electrode distance and height. Methane conversion is a rising function of the power level with a maximum of 65% at about 180 W. The hydrogen yield increases with the power level too, reaching a maximum of about 25%. The global effect of the different electrode configuration is minor at the same power level. Indeed, taking into account that the residence time is more than doubled comparing the two configuration, the efficiency, although a bit higher, is almost unchanged. Therefore, the influence of the gap distance looks quite limited.

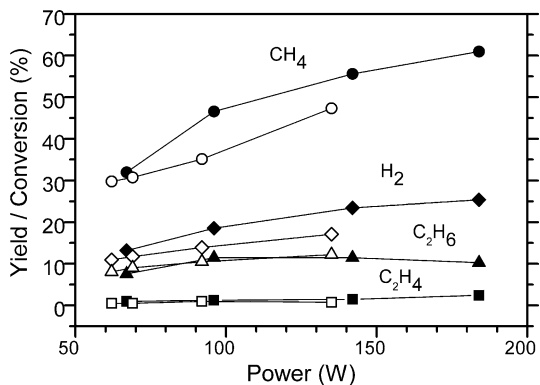
The rest of the gas-phase mainly contains ethane (C<sub>2</sub>H<sub>6</sub>). This again rises as the power level increases. However, the increment is smaller (between 8 and 12%) and, moreover, almost the same for the two electrode configurations. Other hydrocarbons are minor, less than a few percent at maximum, and C<sub>2</sub>H<sub>4</sub> seems to be the most abundant among those. At the maximum power, the gas-phase was composed by 35% methane, 50% hydrogen, 12% C<sub>2</sub>H<sub>6</sub> and 3% other hydrocarbons (2.4% C<sub>2</sub>H<sub>4</sub>).

Another way to look at these data is to calculate the ratio between half the hydrogen amount produced and that of methane destroyed. This is sometimes referred as to selectivity,  $S_{H_2}$  [30]:

$$S_{H_2}(\%) = \frac{1}{2} \cdot \frac{\text{moles of } H_2 \text{ out}}{\Delta(\text{moles of } CH_4 \text{ in} - \text{moles of } CH_4 \text{ out})} \cdot 100 \tag{3}$$

It varies between 35 and 40% and it results to be almost independent of the power level and the electrode configuration. It is also possible to estimate the fraction of power

**Fig. 3** Yields (conversion fraction for methane) estimated from the gas-phase composition as a function of the discharge power level. Full and open points refer to two different configurations, the former to a discharge gap of 3.5 mm with an electrode height of 100 mm whereas the latter to a discharge gap of 2 mm with an electrode height of 80 mm



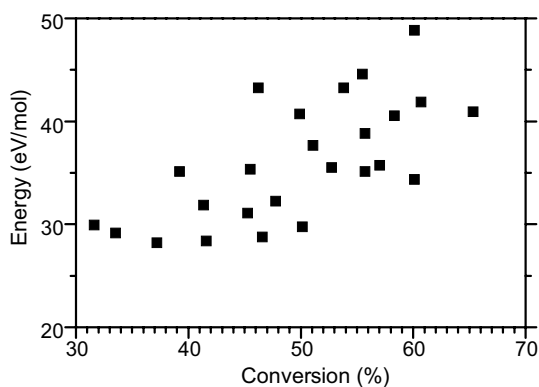
necessary to convert each methane molecule in the reactor. This represents the energy cost of methane conversion.

$$E_{CH_4}(eV) = \frac{W_{plasma}}{Flux(CH_4in) \cdot N_0 \cdot X(CH_4)} \quad (4)$$

where  $N_0$  is the so-called Loschmidt number, that is the gas density at STP. When such cost is plotted as a function of the methane conversion percentage, any difference due to the configuration or power level is cancelled. Data show a rough increase, within a large scatter, from about 30 eV/molecule as the conversion rises above 50% to a range of about 35–50 eV/molecule at higher conversion levels (Fig. 4). It is also possible to estimate the energy cost for the production of each molecule of any species detected in the outgoing gas-phase. In particular we are interested in the energy cost for the production of hydrogen, which turns out to be slightly larger than the energy for methane conversion, as expected because of the reported incomplete selectivity. Another test has been performed by comparing at the same power level three different configurations by changing the external electrode height between 40 and 100 mm, with the same gap distance. The results are shown in Fig. 5 as a function of the residence time in the discharge. The trend is fairly linear, showing the increase of the hydrogen yield (maximum 23%) and of the methane conversion (maximum 54%) with an energy cost of 36 eV per methane molecule and 43 eV per hydrogen molecule. A somewhat comparable increase in the efficiency could be obtained by decreasing the flow velocity (enlarging the electrode gap). Here, this is achieved by reducing the internal electrode diameters. Both trends also suggest the possibility for the search of better operating conditions.

The last point that is worth mentioning concerns the carbon production. Indeed, part of methane is converted into carbon and is deposited on the inner electrode surface facing the outer one and on the quartz tube. The two layers were remarkably different. The internal electrode surface is covered by a black, dusty film very similar to graphite or carbon black. The film on the quartz surface was dark and oily, fairly described as tar-like. This was confirmed by FT-IR ATR spectra of the film samples. The first deposit spectrum in 4000–500  $\text{cm}^{-1}$  range is very similar to the graphite one, with any signal from C–H bonds almost absent. The second film spectrum shows many absorption bands corresponding to C–H bond and to alkanes and alkenes compounds with minor aromatic carbon groups. Although the film thickness changes along the discharge region for both deposits,

**Fig. 4** Energy cost of methane conversion as a function of the conversion fraction





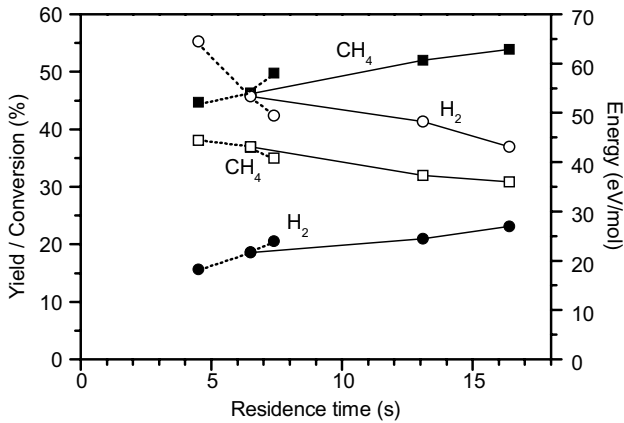


**Fig. 5** Hydrogen yield and methane conversion fraction (full points) as a function of the residence time in the discharge at 145 W power level. The energy cost for each molecule (open points) is displayed too. Dotted lines join points where the electrode distance is increased whereas full lines join points whose rising residence time is due to an increased electrode height

their main composition remains mostly the same. Interestingly, carbon deposition occurs mainly on the dielectric surface, in the lower electric field side, towards the negative polarity electrode, where the recombination process of positive ions from the discharge current may occur. Various tests indicated that hydrogen yield was not significantly affected by pre-heating the gas phase, by the adoption of both a continuous/meshed outer electrode and a rough/smooth inner electrode.

We now turn to discuss the second set of experiments. Here, the DBD is fed by a sinusoidal voltage. Under such operating conditions, the electrical current flowing into the circuit displays the superimposition of a low frequency displacement (capacitive) current, which turns out to be almost independent of the presence of plasma in the gap, and a discharge current, which, when sampled with a suitable fast diagnostics (nanoseconds resolution), appears to be composed of a large number of independent micro-discharge events. The discharge itself reveals to be composed of micro-discharges which are concentrated in two separated active strokes during the oscillation period [25, 31]. As discussed above, Rogowski coils could be used to separate and reconstruct only the micro-discharge current events, which are displayed for the positive stroke in Fig. 6, together with the HV signal for a typical discharge in Ar/CH<sub>4</sub> mixture. It is remarkable that the individual properties of the micro-discharges are only slightly affected by the power level increase. The distribution of amplitude and duration of the micro-discharges are shown in Fig. 7a, b respectively. The two strokes are very similar apart from the reversal in the current sign, despite the electrodes somewhat asymmetric layout. Amplitude distribution is peaked at about 32 mA, with a tail towards larger values. The current pulses duration peaks around 20 ns, with a longer secondary population possibly including also a fraction due to multiple micro-discharges events superposition.

The inspection of the discharge OES spectra shows the dominance of the argon 2p-system, at wavelength above 650 nm. However, the lower wavelengths of the visible range contains also a few interesting details. By increasing the amount of collected light, it is possible to spot some weaker emission lines (see Fig. 8), among whom the most prominent ones turn out to be those of CH and C<sub>2</sub> radicals, as already seen in methane spark

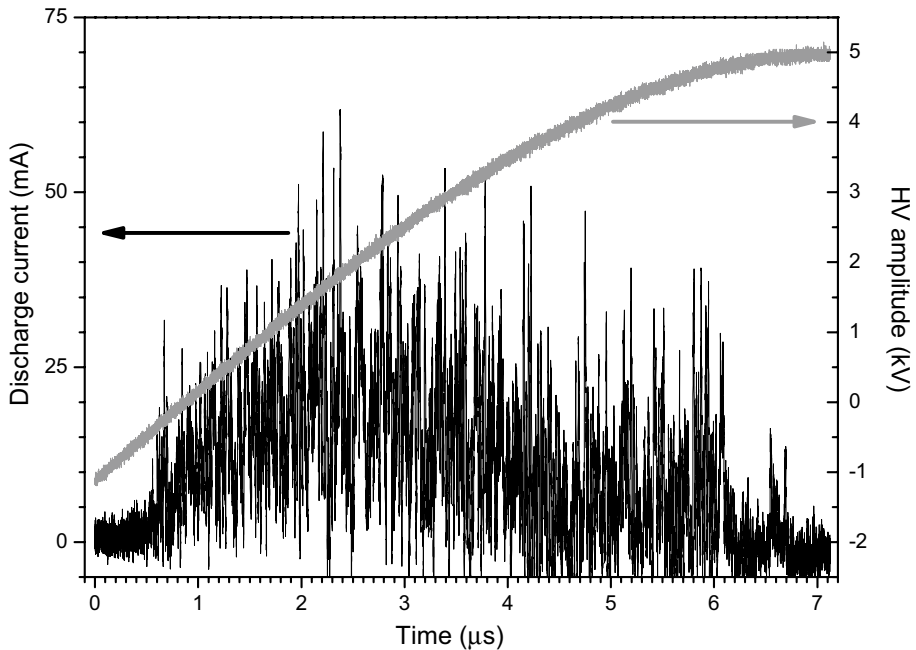


**Fig. 6** Voltage and discharge current spikes recorded during the positive stroke of a 5%  $\text{CH}_4/\text{Ar}$  mixture, 100 W power DBD

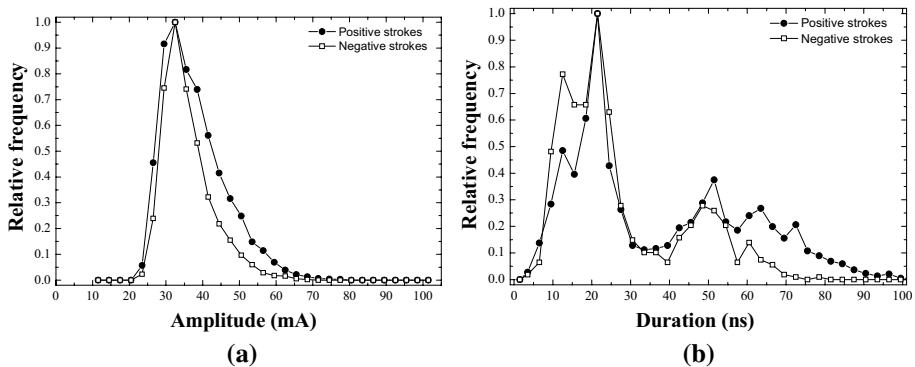


**Fig. 7** Distribution of amplitude (a) and duration (b) of microdischarges recorded during the same 5%  $\text{CH}_4/\text{Ar}$  mixture, 100 W power DBD

discharges [11]. This could be expected, because both species are known to be among the most optically active among hydrocarbon radicals. The main difference in the present experiments is the almost complete absence of atomic hydrogen emission lines, which, on the contrary, are readily observed in spark discharges [11]. The presence of CH and  $\text{C}_2$  radicals demonstrates the deep dissociation of methane and the path towards the formation of higher hydrocarbons, which could bind less hydrogen with respect to methane molecules. This bodes well for hydrogen production, together with the observation that hydrogen

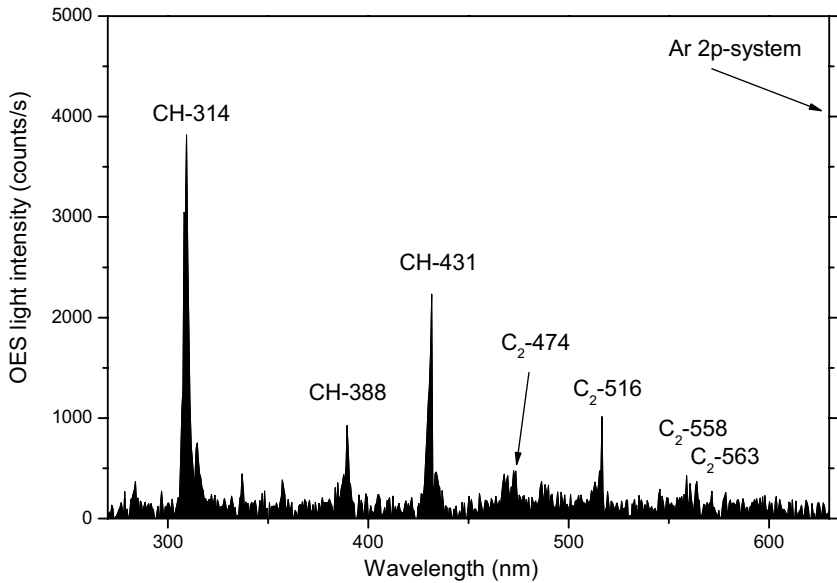


**Fig. 8** Part of the UV–Vis light spectrum of a 5% CH<sub>4</sub>/Ar mixture, 100 W power DBD, showing in particular the emission lines of excited CH and C<sub>2</sub> molecules

atoms are quickly reacting and gets removed from the discharge gas-phase, with little if none emission in this highly diluted methane mixture with argon. Although not so optically active, H<sub>2</sub> molecules were unsuccessfully searched in the spectra too. The near complete absence of OH and N<sub>2</sub> emission, readily observed in OES spectra of DBD [25], demonstrates that air residual and out-gassing are negligible in the reactor gas-phase. Lack of evidence for CO and O emission in the spectra rules out any oxidation of hydrocarbons in the discharge too. The presence of a rich pattern of argon emission lines was used also to estimate the electron temperature in the discharge, using a radiative model, already discussed in our previous work [32]. By taking all the possible ratio between a set of 2p-system lines (here 19 lines), whose excitation rate is slightly dependent on the electron temperature, it is possible to minimize a  $\chi^2$  function and to extract a value of the electron temperature:

$$\chi^2 = 2 \cdot N \cdot (N - 1) \sum_{n < m = 1, N} [\log^2 (R_n / R_m)], \tag{5}$$

$$R_n = (I_n / b_n) / \left[ k_n(T_e) \left( 1 - \sum x^* \right) + \sum k_n^*(T_e) x^* \right]. \tag{6}$$

where  $I_n$  and  $b_n$  are the measured intensities and branching ratios of each emission line considered, whereas the denominator account for the excitation probabilities of the emitting excited state from ground state as well as metastable argon atoms [32]. Using the OES spectra, we could estimate an electron temperature of about  $2.5 \pm 0.5$  eV both in pure argon and in diluted methane mixture discharges. This results only slightly dependent on the power level as well as on the actual percentage of methane (5% maximum).

Finally, we have investigated hydrogen production. Because of the large volume of the reactor chamber with respect to the discharge region and the high dilution of the gas-phase,

we could not reach impressive conversion levels. Indeed, we obtained a hydrogen concentration of 7340 ppm after a 10 min treatment at a power level of 100 W. This corresponds to a yield of 7.34%, and an energy cost of about 40 eV per hydrogen molecule. This is of the same order of magnitude reported in the first set of experiments in pure methane. Thus, dilution is compensated by the higher efficiency of conversion. In general, the yield was nicely linear with the processing time, without any hint of a saturation up to 10 min, This could be inferred from the data in Fig. 9. Other trends could be inferred also by the few data shown in Fig. 9. In particular both higher hydrogen dilution and higher power levels increase the conversion yield. The energy cost can be reduced by acting on the duty-cycle to decrease the total energy absorbed by the discharge. An example is also shown for comparison in Fig. 9. We have obtained a minimum energy of about 30 eV with a duty-cycle of 15%. The benefit arises possibly by letting molecular hydrogen be formed in the gas-phase and diffuse away, before getting involved and partly dissociated in subsequent discharge events.

## Numerical Simulations

Before discussing further our results, we introduce another topic. We tried to get a better insight concerning the reported results by investigating the chemical kinetics in the gas-phase of a methane plasma. This could be done by means of a numerical simulation of the chemical reactions in the plasma gas-phase and of the interactions with the electrode surfaces surrounding the discharge [33–35]. We have already discussed the chemical kinetics of argon/methane mixtures in spark discharges previously [36] as well as the modeling of DBD plasmas in the case of an air gas-phase [37, 38]. So we have modified our programs in order to perform a set of numerical simulation aimed at studying the chemical

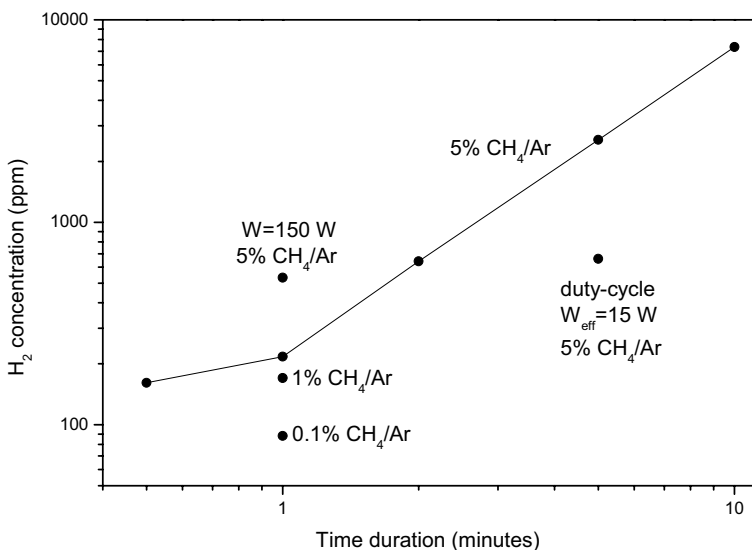


**Fig. 9** Hydrogen concentration reached in the final gas-phase as a function of processing time. The continuous line refers to a 5% CH<sub>4</sub>/Ar mixture and 100 W power. Other operating conditions are reported on the plot for comparison

kinetics of a DBD in an argon diluted methane mixture. Only a few details are discussed here. From the chemical kinetics point of view, the process can be modeled as a very brief phase (less than the typical microdischarge duration) during which energetic electrons produce ions and atomic radicals, followed by a phase in which electrons cool down almost instantaneously, thus ending the dissociation process. The ionizing wave was modeled as propagating straight in the gap between the electrodes, with a circular cross-section, here considered with a diameter  $100\ \mu\text{m}$  as in Ref. [37]. The cylinder height equals the electrode gap in order to match with the performed experiments. The ionizing wave was assumed as a square pulse shape of the electric field strength in the head of the streamer, characterized by the electric field amplitude  $E_{\text{max}}$  and by its time duration, here  $1\ \text{ns}$  [37], which corresponds to an electron temperature of the order of the one measured experimentally and cited above. In general the gas-phase composition in the reactor is determined by the chemical reactions among the reactive species and the transport processes outside/inside the discharge region. The concentration of the different  $N$  species in the gas phase only depends on time and it can be calculated by integrating each balance equation for the density  $n_k$  of the  $k$ th species:

$$\frac{dn_k}{dt} = \sum_{i < j = 1}^N K(i + j \rightarrow k) n_i n_j - \sum_{i, j = 1}^N K(k + i \rightarrow j) n_k n_i - (D_k / \Lambda_k^2) n_k \quad (7)$$

where  $K$  are the reaction rates for the gas-phase reactions including those involving electrons and ions, whereas  $D$  and  $\Lambda$  are the diffusion coefficient and radial scale length [20, 37]. A set of 38 species and 553 reaction rates was included in this calculation. When a single discharge is repeated at a fixed frequency at some tens of kHz, the interplay between the methane dissociation with subsequent production of hydrogen atoms and the reactions in gas phase leading to the molecular hydrogen formation must be considered. After a very small number of repetitions, in the order of ten, the gas-phase reaches a steady composition during the time between each discharge. In order to simulate the real experimental conditions, we have initially exploited the plug-flow reactor approximation. Each gas-phase volume moves along the streamlines approximately without mixing, thus the time evolution of its composition could be translated into the one along the reactor linear streamlines until it reaches the exit. The high discharge repetition rate ensures substantial charge spatial uniformity in the gas flow cross-section. This can be achieved by assuming a slowly varying spatial pattern of subsequent discharges covering the whole electrode gap region. Assuming a size of the ionizing wave of the order reported above, with an experimental frequency of  $18\ \text{kHz}$  and a flow speed of  $9\ \text{mm/s}$ , we get a repetition of discharges every  $10\ \text{ms}$  during the total residence time of  $9\ \text{s}$ . The electron density can be roughly estimated from the total charge transported by the discharge current (shown in Fig. 2) and the assumed size of the ionizing wave channel, in the order of  $10^{15}\ \text{cm}^{-3}$ . A typical plot showing the evolution of the discharge gas-phase is displayed in Fig. 10. Apart from the details of the gas-phase evolution, the final result is a substantial conversion of methane, here about  $33\%$  into mainly molecular hydrogen, reaching a yield of about  $12\%$ . This is also not very far from the experimental reported yield of  $20\%$ . There is also no sign in the simulation preventing an even larger conversion by increasing the residence time or the effective discharge repetition frequency, provided that the same discharge parameters can be maintained. After a few tenths of seconds, the main hydrocarbon produced becomes the  $\text{C}_2\text{H}_6$ . Other stable hydrocarbons such as  $\text{C}_2\text{H}_2$ ,  $\text{C}_2\text{H}_4$ ,  $\text{C}_3\text{H}_x$  and  $\text{C}_4\text{H}_x$  are formed too, but stay minority. This poses a limitation on the achievable hydrogen yield. The simulation clearly shows that the

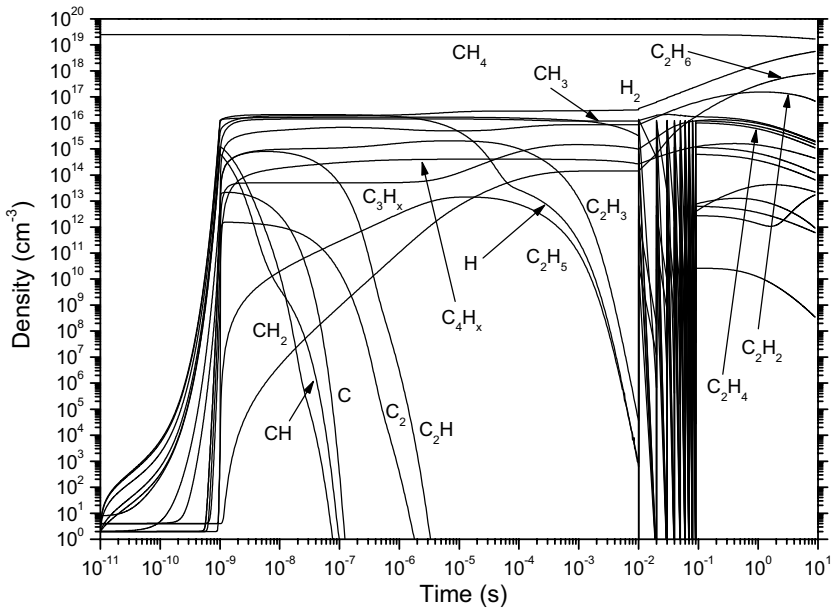


**Fig. 10** Simulation of the evolution of the neutral gas-phase of a methane plug-flow exposed to pulsed discharges with a 100 Hz effective frequency,  $10^{15} \text{ cm}^{-3}$  electron density and 2.5 eV electron temperature ionizing wave. For a better visualization, after 0.1 s, the fluctuations of radical densities are removed from the plot

main dissociation mechanism in a DBD involves methyl radicals  $\text{CH}_3$  and hydrogen atoms  $\text{H}$ . This initial level of dissociation, 1 ns after the end of the ionizing wave, controls the amount of methane conversion together with the effective discharge repetition rate. As the residence time is artificially increased, methane is completely consumed and higher yields are reached, as shown in Fig. 11. In particular the final yield in each volume of the gas-phase turns out to be independent from the discharge frequency and to be proportional to the integrated value of the electron charge density (or, that is the same, the number of free electrons) created in such volume. It is also apparent from the data shown in Fig. 11 that higher yields approaching total conversion require much larger electron densities, which translates in higher energy costs. The final state now contains mainly  $\text{C}_3\text{H}_x$  and  $\text{C}_4\text{H}_x$  species. The actual figure of the yield ( $Y = 63.7\%$  after 64 s, using our standard parameters) however depends on poorly known aspects of the simulation, such as the actual amount of hydrogen trapped in the heavier hydrocarbons and in the carbonaceous deposit at the reactor surfaces. Although the details about the final gas-phase concentrations depend also on the plasma parameters such as the electron temperature and density, the main pattern is quite solid and leads to the prediction of a limited conversion of the available hydrogen atoms. So other methane dissociation patterns are worthy the investigation, such as argon dilution [17]. In order to ease the comparison, we have simulated a discharge with the setup of the first set of experiments, with exactly the same plasma characteristics as the previous one, even if this is clearly a simplification of the real experimental conditions. The corresponding plot showing the evolution of a 5%  $\text{CH}_4/\text{Ar}$  discharge gas-phase is displayed in Fig. 12. As we have observed in spark discharges, a high dilution with argon improves the

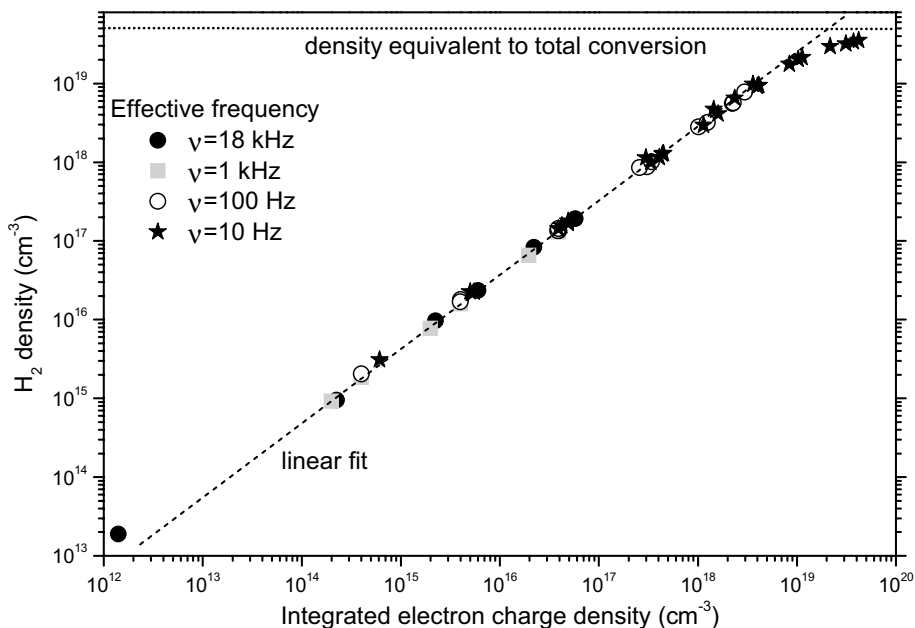


**Fig. 11** Hydrogen density in the final gas-phase as a function of the integrated electron charge density created in the unit volume, for different effective frequencies and residence times

conversion. About 82% of the initial methane molecules is predicted to get transformed. Correspondingly, the hydrogen yield is about 45%. Notwithstanding many differences, which we plan to discuss in a separate paper, the overall trend concerning hydrogen production is similar. The presence of argon in the discharge shifts the balance among different methane dissociation channels. In this case, the initial amount of carbon atoms gets transformed into heavier hydrocarbons molecules with a lower hydrogen contents. Then, a larger quantity of hydrogen atoms are abstracted from methane and transformed in molecular hydrogen. This prediction needs to be confirmed since the modeling can simulate such process only up to C<sub>4</sub>H<sub>x</sub> radicals, but it seems substantially robust and reliable.

## Discussion of Results and Conclusions

In some sense, the use of single HV pulses as the source for DBD is the most straightforward, since it allows to detail a specific process recipe. Each discharge could be understood as a repetition, the most faithful available, of the previous one. Provided the HV pulse duration is fast and followed by a suitable interval of quiet, the power level is small, as well as the heating of the gas-phase. Moreover, we can assume that each discharge is not much influenced by the previous ones. In the end, the pulse shape can be optimized in amplitude, polarity and duration in order to achieve the highest conversion yields. However these characteristics of the source represent also the most obvious drawbacks. Even if the repetition frequency could be increased, the discharge is for the most of the time off. This saves power but also decreases the throughput, slowing down or decreasing the conversion.

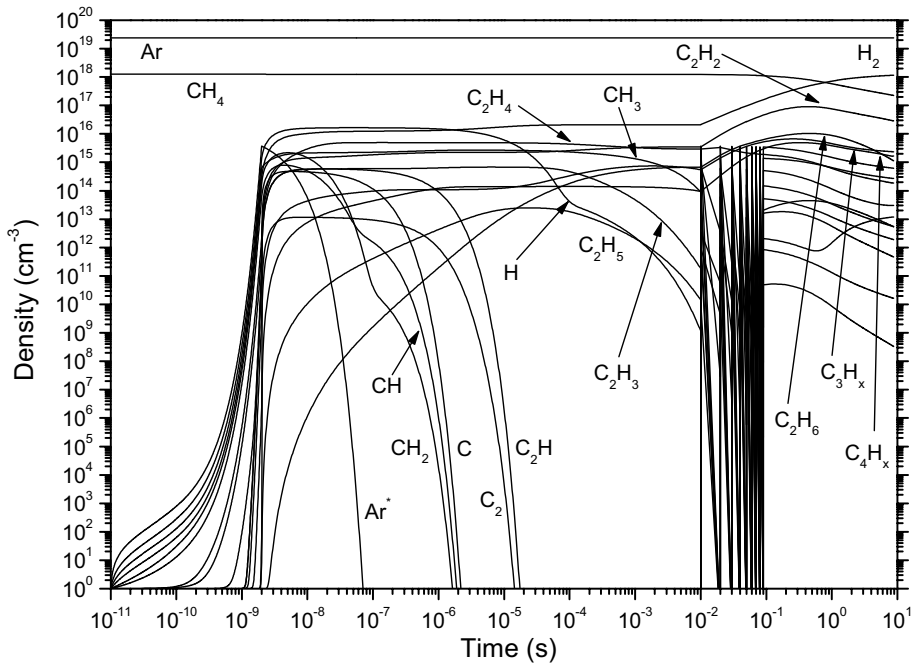


**Fig. 12** Simulation of the evolution of the neutral gas-phase of a 5% methane in argon plug-flow exposed to pulsed discharges with a 100 Hz effective frequency,  $10^{15} \text{ cm}^{-3}$  electron density and 2.5 eV electron temperature ionizing wave. For a better visualization, after 0.1 s, the fluctuations of radical densities are removed from the plot

Another issue regards the uniformity of treatment. There might be regions where breakdown is less likely to occur and the gas flowing through them gets a different, presumably less efficient treatment. Even if each single discharge could “spread” somewhat in the gap volume, the overall electron density is small and so is the methane conversion.

On the other hand, the use of a continuous varying HV signal, a sinusoidal being the most easy and common implementation, could help in this direction. Because of the voltage variations and of the charges left in the gap or at the dielectric surfaces, the discharges cannot be all similar. Indeed, the DBD could be understood as the effect of a population of discharges, each with its own individual characteristics. Generally, using similar HV amplitudes and electrodes as those of a single pulse source, the power level is high and the gas heating could become not negligible, favouring mixing. In this case, uniformity of treatment of the gas-phase is more easily achieved, also because the accumulation of charges in the previous discharges usually prevents the formation of stable spatial pattern of microdischarges.

In both cases, however, the discharge pattern in methane is determined by the chemical kinetics dictated mainly by the initial dissociation provided by electron impact. Although electron temperature and density, together with the gas temperature, the repetition frequency and the diffusion timescales all have some control on the gas-phase evolution, the main consequences of the chemical kinetics cannot be escaped. The rapid formation of H/CH<sub>3</sub> pairs and their subsequent reaction pattern, leads to molecular hydrogen formation. However, the competing reaction producing higher hydrocarbons sequesters a non



negligible amount of the initial hydrogen atoms. We have suggested, starting from some experimental evidence and evidences from numerical simulations of DBD plasma chemical kinetics, that a different pattern of dissociation could be opened by a substantial dilution of the initial gas mixture with a noble gas such as argon. The main advantage lies in the preferential formation of higher hydrocarbons with low hydrogen contents, thus freeing more hydrogen atoms from carbon bonds. Argon dilution could also possibly help in the stabilization and the leveling out of electrical discharges, being unaffected by the evolution of the gas-phase composition.

Our experiments show that high methane conversion could be achieved by pulsed DBD. Conversion as high as 60%, together with hydrogen yield that could reach about 25%, with energy costs in the range 30–40 eV per molecule. The experiments with the sinusoidal DBD reactor in highly diluted argon/methane mixtures, show that similar energy costs could be achieved, notwithstanding the much smaller amount of hydrogen atoms available. However, under our experimental conditions the hydrogen yield remained limited, under 10%. Numerical simulations of the chemical kinetics of DBD plasmas could be performed with a fair degree of confidence. Yields similar to those reported in the experiments in pure methane pulsed DBD were predicted. Numerical simulations of argon/methane plasmas have been performed too. They provide a possible path leading to higher conversion rate with improved selectivity towards hydrogen.

As a final remark, we do believe that DBDs represent a viable possible choice for plasma hydrogen reforming: methane conversion is not restricted to hot plasma sources but could be achieved even remaining strictly within the non-thermal plasma conditions. It should be noted, however, that the energy costs, which we estimated in the order of 450–600 kJ/g of hydrogen produced, are yet much larger than those reported with other technologies [4].

## References

1. Dutta S (2014) *J Ind Eng Chem* 20:1148
2. Mazloomi K, Gomes C (2012) *Renew Sustain Energy Rev* 16:3024
3. Edwards PP, Kuznetsov VL, David WIF, Brandon NP (2008) *Energy Policy* 36:4356
4. Dutton AG (2003) *Wind Eng* 27:239
5. Lide DR (2007) *CRC handbook of chemistry and physics*, 88th edn. CRC Press, Boca Raton
6. Aasberg-Petersen K, Bak Hansen JH, Christensen TS, Dybkjaer I, Seier-Christensen P, Stub-Nielsen C, Winter-Madsen SEL, Rostrup-Nielsen JR (2001) *Appl Catal A* 221:379
7. Crabtree GW, Dresselhaus MS, Buchanan MV (2004) *Phys Today* 57:39
8. Fridman A (2008) *Plasma chemistry*. Cambridge University Press, Cambridge
9. Lesueur H, Czernichowski A, Chapelle J (1994) *Int J Hydrog Energy* 19:139
10. Sekiguchi H, Mori Y (2003) *Thin Solid Films* 435:44
11. Barni R, Quintini A, Piselli M, Riccardi C (2008) *J Appl Phys* 103:063302
12. Shapoval V, Marotta E, Ceretta C, Konjevic N, Ivkovic M, Schiorlin M, Paradisi C (2014) *Plasma Proc Polym* 11:787
13. Paulmier T, Fulcheri L (2005) *Chem Eng J* 106:59
14. Cormier JM, Rusu I (2001) *J Phys D* 34:2798
15. Bromberg L, Cohn DR, Rabinovich A, Alexeev N, Samokhin A, Ramprasad R, Tamhankar S (2000) *Int J Hydrog Energy* 25:1157
16. Kogelschatz U (2003) *Plasma Chem Plasma Proc* 23:1
17. Riccardi C, Barni R, Fontanesi M, Tosi P (2000) *Chem Phys Lett* 392:66
18. Muller S, Zahn RJ (2007) *Contrib Plasma Phys* 47:520
19. Spinicchia N, Maffi S, De Angeli M, Gervasini G, Nardone A, Zizak G (2012) I.F.P. Internal Report FP12/02
20. Chantry PJ (1987) *J Appl Phys* 62:1141
21. Benson SW (1982) *Thermochemical kinetics*. Wiley, New York

22. Siliprandi RA, Zanini S, Grimoldi E, Fumagalli F, Barni R, Riccardi C (2011) *Plasma Chem Plasma Proc* 31:353
23. Barni R, Biganzoli I, Dell'Orto EC, Riccardi C (2015) *J Appl Phys* 118:143301
24. Argueso M, Roble G, Sanz J (2005) *Rev Sci Instrum* 76:065107
25. Biganzoli I, Barni R, Riccardi C, Gurioli A, Pertile R (2013) *Plasma Sources Sci Technol* 22:025009
26. Biganzoli I, Barni R, Riccardi C (2013) *Rev Sci Instrum* 84:016101
27. Laux CO, Spence TG, Kruger CH, Zare RN (2003) *Plasma Sources Sci Technol* 12:125
28. Barni R, Riccardi C (2018) *Europ Phys J B* 72:62
29. Zielinski WL (1987) *CRC handbook of chromatography*. CRC Press, Boca Raton FL
30. Li X-S, Zhu A-M, Wang K-J, Xu Y, Song Z-M (2004) *Catal Today* 98:617
31. Siliprandi RA, Roman HE, Barni R, Riccardi C (2008) *J Appl Phys* 104:063309
32. Crococolo F, Barni R, Zanini S, Palvarini A, Riccardi C (2008) *J Phys Conf Ser* 100:062023
33. Sommerer TJ, Kushner MJ (1992) *J Appl Phys* 71:1654
34. Font GI, Morgan WL, Mennenga G (2002) *J Appl Phys* 91:3530
35. Rehman F, Lozano-Parada JH, Zimmerman WB (2012) *Int J Hydrog Energy* 37:17678
36. Barni R, Broggi C, Benocci R, Riccardi C (2006) *Eur Phys J Appl Phys* 35:135
37. Barni R, Esena P, Riccardi C (2005) *J Appl Phys* 97:073301
38. Patel V (2012) *Chemical kinetics*. Intech, Rijeka